Acoustic Fatigue Design Information for Honeycomb Panels with Fiber-Reinforced Facings

M. J. JACOBSON*
Northrop Corporation, Hawthorne, Calif.
AND
R. C. W. VAN DER HEYDE†
Air Force Flight Dynamics Laboratory, Wright-Patterson Air Force Base, Ohio

This paper is concerned with portions of an extensive analytical and experimental program that was formulated to obtain acoustic fatigue design information for fiber reinforced structure. Fiber-reinforced structure is expected to see increasing use in aircraft because of its favorable strength–weight ratio, and acoustic fatigue design information for such structure is needed. Panel design, stress data, panel lifetime, and modes of failure are reported from acoustic tests of honeycomb panels, mainly with S-glass fiber-reinforced facings, but also with boron fiber-reinforced facings and with aluminum alloy facings. Facing failures near the panel center predominated. When failure occurs in the facings near the panel center, the predicted panel life, based on the Rayleigh–Miner hypothesis, is compared with experimental life for panels with S-glass fiber-reinforced facings. The effects of angle-plied facings, cross-plied facings, and parallel-plied facings on the panel life and mode of failure are reported. In addition to providing acoustic fatigue design information, this program has demonstrated that high-quality honeycomb panels with S-glass fiber and boron fiber-reinforced facings can be designed and fabricated to offer greater resistance to acoustic loading than well-designed and well-fabricated aluminum honeycomb panels of comparable weight and thickness.

Nomenclature

BFR = boron fiber-reinforced
D_i = the logarithmic deviation from the logarithmic mean to failure of the ith specimen
db = decibels (re 0.0002 dynes/cm^2)
K = constant
N = the computed kilocycles to failure corresponding to the confidence and survival levels
$\bar{N}$ = the logarithmic mean of kilocycles to failure of the specimens
n = the number of specimens
S901/43L = parallel-plied S901/43 longitudinal fatigue coupons
S901/81L = parallel-plied S901/81 longitudinal fatigue coupons
S901/43T = parallel-plied S901/43 transverse fatigue coupons
S_L = stress in warp direction of SGFR plies and in filament direction of BFR plies
S_T = stress in fill direction of SGFR plies and in transverse directions of BFR plies
SGFR = S-glass fiber-reinforced
SPL = sound pressure level

Subscripts

$-EX$ = experimental
$-TH$ = theoretical

Introduction

THE work reported here on honeycomb panels with S-glass and boron-reinforced facings (hereafter designated SGFR and BFR, respectively) was part of a larger program[1] directed towards the general objective of developing acoustic fatigue design information for glass and boron fiber-reinforced materials. Acoustic fatigue design information for these materials has been generally unavailable. The over-all test and analytical programs[1] included the following phases: 1) fabricating and testing under discrete frequency or random acoustic loading three aluminum honeycomb panels, forty-six honeycomb panels with S901/81 or S901/43 facings, and twelve honeycomb panels with boron fiber-reinforced facings; 2) fabricating and testing fatigue coupons of S901/81 and S901/43 SGFR material under fully reversed, discrete frequency, uniaxial loading; 3) fabricating S901/81 and S901/43 SGFR coupons and conducting tests to obtain physical and mechanical properties; 4) developing theory and a related computer program to predict natural frequencies, stresses, and lives of sandwich panels with orthotropic cores and thin fiber-reinforced facings; 5) analyzing the test and analytical results and presenting the results in a readily usable form to a designer.

This paper covers portions of the over-all program concerned with panel lifetime and modes of failure in the acoustic tests. Acoustic fatigue design criteria for fiber-reinforced structure are in a formative stage, and qualitative information presented in this paper can be used as design guidelines at the present level of the state-of-the-art.

Presented as Paper 70–897 at the AIAA 2nd Aircraft Design and Operations Meeting, Los Angeles, Calif., July 20–22, 1970; submitted September 15, 1970; revision received August 9, 1971. This work was supported by the U.S. Air Force, Flight Dynamics Lab., under Contract F33615-67-C-1672.

Index categories: Aircraft Structural Design; Aircraft Structural Materials.

* Engineering Specialist, Aircraft Div., Structures Research and Technology Department Member AIAA.

† Aerospace Engineer, Vehicle Dynamics Div., Aero Acoustics Branch.

Acoustic Test Program

Description

The acoustic test program was formulated to produce data for use in establishing acoustic fatigue design criteria. An overriding item was the fabrication of high-quality, lightweight panels that could be tested to failure in the available progressive wave acoustic test chamber. Based on linear analysis methods and previous test results, the decision was made to fabricate honeycomb panels with two-ply precured fiber-reinforced facings and a 0.200-in. core. Three aluminum honeycomb panels were chosen as control panels. Square panels with over-all dimensions 22 × 22 in. and rectangular panels

with over-all dimensions 30 × 22 in. were chosen to account for different aspect ratios.

Standard materials were used throughout the test program. The Stanpreg 5101 epoxy prepreg system with S901/81 and S901/43 glass fabric was used as facings and doublers in the honeycomb panels with SGFR facings. The other panels with fiber-reinforced facings were fabricated with Narmco 5505 boron tape. Hexagonal cell core was used in all honeycomb panels.

The description of the panels is given in Tables 1 and 2. The ply layup in Table 1 designates the orientation of the glass fabric warp direction relative to the core ribbon direction.

Table 1 Honeycomb panel acoustic test data

Panel designation	Facing description; length by width (A" × B"); ply layup (C^o, D^o)	Total panel weight, lb	Adhesive, lb/ft²	Over-all pressure, db	Test time, min	Failure mode[a]; facing crack length, in.	Propagation time,[b] min
A-1-1	S901/81; 22 × 22; 0,0	2.14	0.03	167 (DF)[c]	2	ADH., U.C.	1
A-1-2	S901/81; 22 × 22; 0,0	2.09	0.03	167 (DF)	0	ADH., U.C.	0
A-1-3	S901/81; 22 × 22; 0,0	2.14[d]	0.03	166 (DF)	12	ADH., U.C.	0
A-1-4	S901/81; 22 × 22; 0,0	2.45	0.08	167.5 (DF)	500	NF	...
A-1-5	S901/81; 22 × 22; 0,0	2.34	0.08	166 (DF)	5	CORE, ADH,; U.C.	0
A-1-6	S901/81; 22 × 22; 0,0	2.34	0.08	167 (DF)	128	F.C., P.C.; 10.5	53
A-2-1	S901/81; 22 × 22; 0,0	2.41	0.08	164 (DF)	30	F.C., DIAG.; 30	20
A-2-2	S901/81; 22 × 22; 0,0	2.32	0.08	164 (DF)	510	NF	...
A-2-3	S901/81; 22 × 22; 0,0	2.21	0.08	164 (DF)	500	NF	...
A-3-1	S901/81; 22 × 22; 0,0	2.14[d]	0.03	161 (DF)	515	NF	...
A-5-1	S901/81; 22 × 22; 0,0	2.14[d]	0.03	167.5 (R)[c]	500	NF	...
A-5-2	S901/81; 22 × 22; 0,0	2.14	0.03	167.5 (R)	5	ADH., U.C.	0
A-5-3	S901/81; 22 × 22; 0,0	2.38	0.08	167.5 (R)	500	NF	...
B-1-1	S901/81; 30 × 22; 0,0	3.33	0.08	165 (DF)	500	NF	...
B-1-2	S901/81; 30 × 22; 0,0	3.08	0.08	165 (DF)	11	ADH(C), DZLS	0
B-1-3	S901/81; 30 × 22; 0,0	3.26	0.08	165 (DF)	500	NF	...
B-4-1	S901/81; 30 × 22; 0,0	3.22	0.08	166 (R)	530	ECC	30
B-4-2	S901/81; 30 × 22; 0,0	3.21	0.08	166 (R)	500	ECC	0
B-4-3	S901/81; 30 × 22; 0,0	3.08	0.08	166 (R)	306	RCWCG	40
C-1-1	S901/81; 30 × 22; −15,15	3.16	0.08	164.5 (DF)	500	NF	...
C-4-1	S901/81; 30 × 22; −15,15	3.11	0.08	166 (R)	500	ECC; 16	0
C-4-2	S901/81; 30 × 22; −15,15	3.08	0.08	166 (R)	370	ADH(C), DZLS	180
D-1-1	S901/43; 22 × 22; 0,90	2.11	0.03	167 (DF)	12	F.C.; 6	2
D-1-2	S901/43; 22 × 22; 0,90	2.13	0.03	166.5 (DF)	3	ADH., U.C.	2
D-1-3	S901/43; 22 × 22; 0,90	2.02	0.03	167 (DF)	15	F.C., P.C.; 9	0
D-2-1	S901/43; 22 × 22; 0,90	2.15	0.03	167.5 (R)	305	F.C., P.C.; 9	5
D-2-2	S901/43; 22 × 22; 0,90	2.14[d]	0.03	167.5 (R)	690	ADH.(C), UZD	15
D-2-3	S901/43; 22 × 22; 0,90	2.15	0.03	167.5 (R)	390	F.C., FF & FE; 6	0
D-2-4	S901/43; 22 × 22; 0,90	2.12	0.03	167 (R)	3	ADH., LARGE AREA	0
E-1-1	S901/43; 30 × 22; 0,0	3.18	0.08	163.5 (DF)	35	F.C., P.C.; 20	0
E-1-2	S901/43; 30 × 22; 0,0	3.19	0.08	163 (DF)	7	F.C., P.C.; 17	0
E-1-3	S901/43; 30 × 22; 0,0	3.15	0.08	164 (DF)	15	F.C., P.C.; 3	5
E-2-1	S901/43; 30 × 22; 0,0	3.19	0.08	166 (R)	150	F.C., P.C.; 20	0
E-2-2	S901/43; 30 × 22; 0,0	3.16	0.08	166 (R)	135	F.C., P.C.; 20	5
E-2-3	S901/43; 30 × 22; 0,0	3.14	0.08	166 (R)	160	F.C., P.C.; 19	10
F-1-1	S901/43; 30 × 22; −45,45	3.20	0.08	162 (DF)	500	NF	...
F-1-2	S901/43; 30 × 22; −45,45	3.28	0.08	163 (DF)	500	NF	...
F-2-1	S901/43; 30 × 22; −45,45	3.19	0.08	166 (R)	500	NF	...
G-1-1	S901/43; 30 × 22; −15,15	3.16	0.08	166 (DF)	320	HPC	45
G-1-2	S901/43; 30 × 22; −15,15	3.11	0.08	163 (DF)	30	CORE, ADH., DZLS	10
G-1-3	S901/43; 30 × 22; −15,15	3.12	0.08	164 (DF)	35	CORE, ADH., DZLS, DZSS	15
G-2-1	S901/43; 30 × 22; −15,15	3.14	0.08	166 (R)	101	ADH.(C), DZLS, DZSS	66
H-1-1	BORON; 22 × 22; 0,0	2.16	0.08	166 (R)	1	F.C., P.C.; 17	0
H-2-1	BORON; 22 × 22; 0,0	2.10	0.08	160 (R)	4	F.C., P.C.; 16	0
H-3-1	BORON; 22 × 22; 0,0	2.16	0.08	154 (R)	500	NF	...
I-1-1	BORON; 22 × 22; 0,90	2.14	0.08	166 (R)	500	NF	...
I-1-2	BORON; 22 × 22; 0,90	2.17	0,08	166 (R)	500	NF	...
I-2-1	BORON; 22 × 22; 0,90	2.14	0.08	166 (DF)	500	NF	...
J-1-1	BORON; 22 × 22; −15,15	2.15	0.08	165 (R)	20	H.I.P.C.	0
J-1-2	BORON; 22 × 22; −15,15	2.20	0.08	166 (R)	13	F.C. LED TO H.I.P.C.	6
J-1-3	BORON; 22 × 22; −15,15	2.18	0.08	165 (R)	20	F.C. LED TO H.I.P.C.	3
K-1-1	BORON; 30 × 22; −20,20	2.92	0.08	166 (R)	500	NF	...
K-1-2	BORON; 30 × 22; −20,20	2.88	0.08	166 (R)	120	F.C., P.C.; 25	50
K-1-3	BORON; 30 × 22; −20,20	2.91	0.08	166 (R)	500	NF	...
L-1-1	ALUMINUM; 22 × 22	2.09	0.03	165 (DF)	4	F.C., P.C.; 11	0
L-2-1	ALUMINUM; 22 × 22	2.06	0.03	167 (R)	150	F.C., P.C.; 12	0
L-3-1	ALUMINUM; 22 × 22	2.10	0.03	160 (DF)	39	F.C., P.C.; 16	0

[a] ADH = adhesive, U.C. = undoubled corner, NF = no failure, F.C. = facing crack, P.C. = panel center, DIAG = crack propagating diagonally across facing from a corner, ADH(C) = adhesive and possible core failure, DZLS = doubler zone (long side), UZD = undoubled zone downstream, FF & FE = downstream junction of a foam filler and flat edge, ECC = edge crack at clamp, RCWCG = a facing encountered repeated contact with a capacitance gage, DZSS = doubler zone short side, H.I.P.C. = hole in panel center.

[b] Time from initial observation of failure mode to end of test.

[c] DF = discrete frequency, R = random.

[d] Estimated.

Table 2 Properties of components of honeycomb test panels

Facing material	S901/81	S901/43	Narmco 5505 Boron tape	2024-T3 clad aluminum
Core thickness, in.	0.200	0.200	0.200	0.200
Facing thickness, in.	0.022	0.022	0.010	0.010
Plies per facing	2	2	2	1
Core material	NP$\frac{3}{16}$ – 112 – 4.5	NP$\frac{3}{16}$ – 112 – 4.5	$\frac{3}{16}$ – 5052 – 0.003	$\frac{3}{16}$ – 5052 – 0.003
Core shear moduli, psi	14,500 5,900	14,500 5,900	129,500 56,500	129,500 56,500
Core weight density, lb/ft^3	4.5	4.5	8.1	8.1
Facing weight density, lb/in.^{3}	0.069	0.069	0.070	0.100
Facing Young's moduli, psi	4.35×10^6 3.95×10^6	6.20×10^6 2.50×10^6	33.3×10^6 3.33×10^6	10.6×10^6 10.6×10^6
Facing shear mdulus	1.68×10^6	1.87×10^6	1.22×10^6	3.96×10^6
Facing Poisson's ratio (larger)	0.12	0.20	0.38	0.34

For example, $-15°$, $15°$ means that the warp direction of the two plies adjacent to the core was colinear and made a $-15°$ angle with the core ribbon direction, whereas the warp direction of the two plies not adjacent to the core was colinear and made a $+15°$ angle with the core ribbon direction. The ply layups reported are 0°, 0°; 0°, 90°; $-15°$, 15°; $-20°$, 20°; and $-45°$, 45°.

The core ribbon direction of all square honeycomb panels (excluding panel A-1-6) and the rectangular boron fiber-reinforced honeycomb panels was in the direction of flow in the progressive wave acoustic test chamber (Fig. 1), whereas the core ribbon direction of the remaining panels of Table 1 was perpendicular to the direction of flow. The length of the rectangular panels and two edges of the square panels were in the direction of flow.

The fabrication method for the honeycomb panels is described in detail in Ref. 1. For honeycomb panels with fiber-reinforced facings, a two-stage procedure was used with the facings cured in the initial stage and bonded to the core in the final stage. The edge detail for the honeycomb panels is shown in Figs. 2 and 3. The additional thickness at the edges contributed by the doublers was sufficient in most instances to prevent panel failures at the test fixture, which held the panels solely by friction.

The initial honeycomb panels were fabricated with a 0.03-lb/ft^2 adhesive bonding the core to the facing. However, the initial honeycomb panels with S901/81 facings experienced adhesive failures at the corners of undoubled edges due to high in-plane shearing stresses. A heavier adhesive weighing 0.08-lb/ft^2 was used for the remaining panels, for which no failures were definitely attributed to the adhesive.

The use of S901/43 fabric for doubler material was used only on a few of the initially fabricated honeycomb panels and was

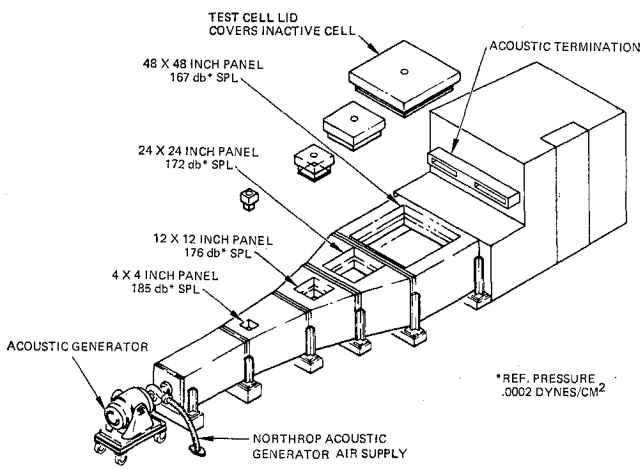

Fig. 1 Progressive wave acoustic test chamber.

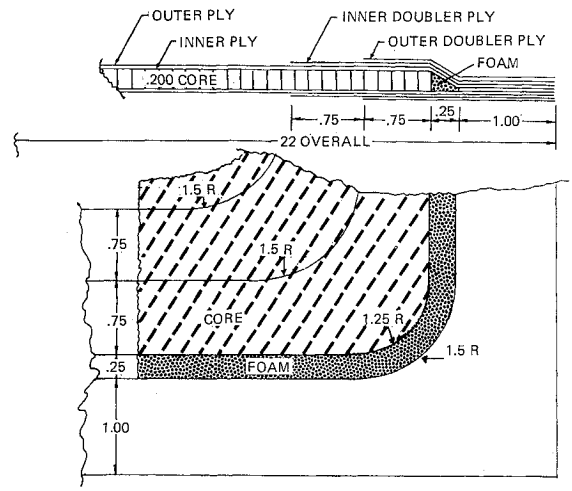

Fig. 2 Edge detail for honeycomb panels with S-glass facings.

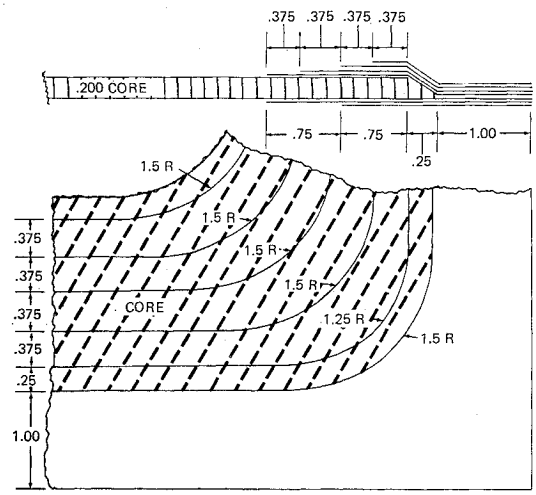

Fig. 3 Edge detail for aluminum and boron honeycomb panels.

discontinued when it was determined that it produced significant nonuniform peripheral loads that adversely affected the lives of the honeycomb panels with S901/81 facings. Panels A-1-2, A-3-1, A-5-2, D-1-2, D-2-3, and D-2-4 were fabricated with S901/43 doublers, and panels L-1-1 and L-2-1 were fabricated with 150/181 E glass fabric doublers. All of the doublers on the remaining honeycomb panels were of S901/81 fabric.

A possible reason for adhesive failures in fabricated panels A-1-2, A-5-2, D-1-2, and D-2-4 was the improper use of silicone

release agent on the mold during cure. The improper use was corrected after its discovery was made.

Acoustic Testing

All acoustic testing was conducted in the Progressive Wave Acoustic Test Chamber of the Northrop Acoustic Test Facility (Fig. 1). The chamber consists of a 16-ft-long 30-Hz exponential horn leading into a constant 4-ft-square × 9-in.-deep test section. The test area is terminated by an acoustical absorber effective above 30 Hz in reducing longitudinal standing waves in the test chamber.

The chamber was driven by the Noraircoustic Generator MK-V-H. The generator, an air-stream modulator driven by a 1500-lbf electro-hydraulic actuator, is capable of providing 50 kw of broadband random acoustic energy, as well as discrete frequency energy. The over-all sound pressure level in the 24 × 24-in. test section reached 168.5 db and in the 48 × 48-in. test section reached 166 db. A discussion of the auto- and cross-correlation of the pressure in the 24 × 24-in. and the 48 × 48-in. test section is in the Appendix.

Discrete-frequency operation of the generator yields a sawtooth wave form at the excitation frequency with accompanying harmonic content in the pressure wave. A narrow-band analysis of a train of the pulses has shown the fundamental frequency plus both even and odd harmonics of the fundamental. The envelope of the harmonics indicates an attenuation rate from the fundamental frequency of 8.5 db per octave. Acoustic power at these harmonic frequencies normally is of a low level and in this program did not appreciably excite higher modes of a panel when driving the panel at its fundamental frequency.

It was impractical to attempt to subject the panels to wide-band random loading in the Northrop Progressive Wave Acoustic Test Chamber that would excite modes other than the fundamental mode at a significant level. Therefore, the acoustic testing was restricted to either discrete frequency excitation or random excitation that primarily excited the fundamental mode (typical random excitation at the 24 × 24-in. test section at 139 db SPL is given in Fig. 4).

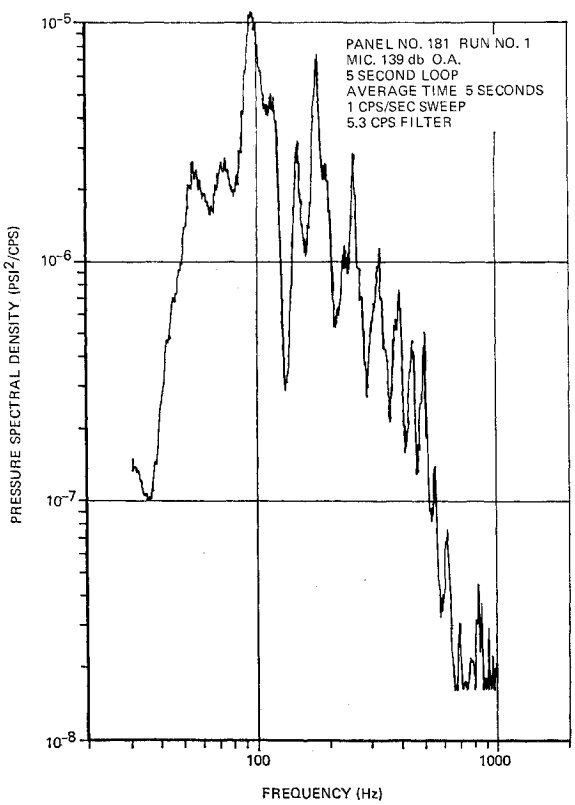

Fig. 4 Typical spectral analysis of acoustic pressure.

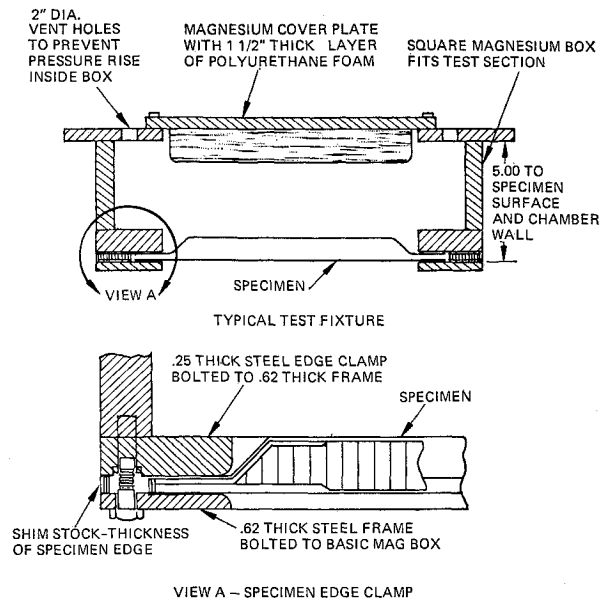

Fig. 5 Test fixture and edge condition.

The test specimens were supported in fixtures replacing either the 24 × 24-in. or 48 × 48-in. test section lids. A schematic of the fixture and a panel is given in Fig. 5. So that sound would impinge on the front face only, the rear side of the panel was enclosed with a box, designed to minimize effects on the damping and stiffness of the panel under the acoustic loading.

The panel boundary conditions were selected after reviewing the practical considerations of fixture design. The fixtures were designed to minimize problems normally associated with a bolted edge-type clamp in which fasteners pass directly through the test specimen edge. The large radius at the edge of the clamp was to reduce stress concentration. The line-on-line fit of the specimen in the clamp allowed deflection of the panel center and return to the original position without "oil canning" encountered with a bolted edge.

All acoustic measurements were made with Photocon Model 524 microphones. The microphone output was obtained from Photocon 605D Dynagages and read on B & K Type 2409 Electronic Voltmeters. The output from EA-13-250-BB strain gages was recorded on one-inch magnetic tape with a Sanborn Model 3914 Tape Recorder. The output was read on a Ballentine Model 320 or 321 True RMS Voltmeter. Analysis of data for power spectral density was made with a Technical Products TP-625 Wave Analyzer. Probability density analysis was performed with a B & K Model 161 Probability Density Analyzer.

The probability density function of the instantaneous strain (Fig. 6) and the positive and negative strain peaks (Fig. 7) were recorded for honeycomb panel P3-181 with S901/81 facings. Panel P3-181 was fabricated for a preliminary acoustic test program to obtain data for the purpose of verifying the usefulness of the designs of the test panels in Table 1 prior to their fabrication. Panel P3-181 was essentially the same as Panel A-1-1.

The instantaneous probability density function (Fig. 6) has a shape much like that of a Gaussian distribution function. The peak probability function (Fig. 7) at zero stress should be decreased by 50% to account for the method of counting strain peaks at the zero stress level. The positive half-plane, as well as the mirror image of the negative half-plane about the vertical axis, resemble, but do not duplicate, the Rayleigh probability density function for rms strain peaks that have been used in some previous fatigue studies as well as in this program.

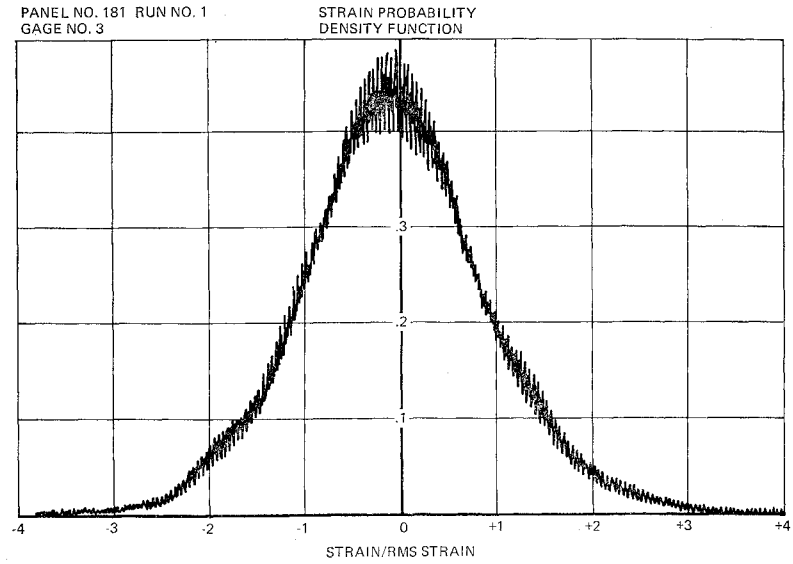

Fig. 6 Probability density function of strain at gage 3 of panel P3-181.

Damping factors were found by the logarithmic decrement method utilizing the oscillograph decay record taken from strain gage signals. A Consolidated Electrodynamics Model 5-124 Recording Oscillograph was used. The damping factors of the square panels were, in general, of good quality, although there was considerable scatter. The damping factors of the rectangular honeycomb panels were, in general, of poor quality with even more scatter than for the square panels. The damping factors (and strain readings) were taken prior to the sonic fatigue test.

A brief description of the discrete frequency test method follows. To obtain a resonant frequency, the sound pressure level was held at a constant value while the loading frequency was swept to obtain a frequency (the resonant frequency) to produce a maximum voltage output from the capacitance probe or the strain gage. The strain gages were used as the primary data source. The strain gages were not sufficiently durable to last more than ten minutes at the maximum sound pressure levels. After the strain gages failed, the capacitance probe was used to monitor the fundamental frequency. The output of the capacitance probe was filtered by a 2Hz band-width tracking filter to eliminate noise and harmonics. Occasionally this procedure did not produce a voltage output that clearly defined the resonant frequency. More reliable tuning, i.e., determination of the natural frequency, could have been achieved from strain gage response; however, the state-of-art is such that strain gages were unavailable for lengthy operation in the high-intensity acoustic environments.

During the course of a 500-min fatigue test, the panel edges would wear due to the clamping, and the fundamental frequency would drift down because of the looser clamp. In an attempt to compensate for the edge wear, the excitation frequency was lowered to retain excitation at resonance, or testing was halted to remove layers of the shims in the edge clamp to provide tight clamping again once testing was resumed. Because of the lower stress and displacement levels, there was less wear of the panel edges in the test fixture in random tests at maximum power than in discrete frequency tests at maximum power.

During acoustic fatigue testing, visual inspections of the panel were performed periodically to determine the initiation and/or propagation of a failure mode. Other effective means of determining the occurrence of failure were an abrupt change in a strain gage signal or sound pressure signal. However,

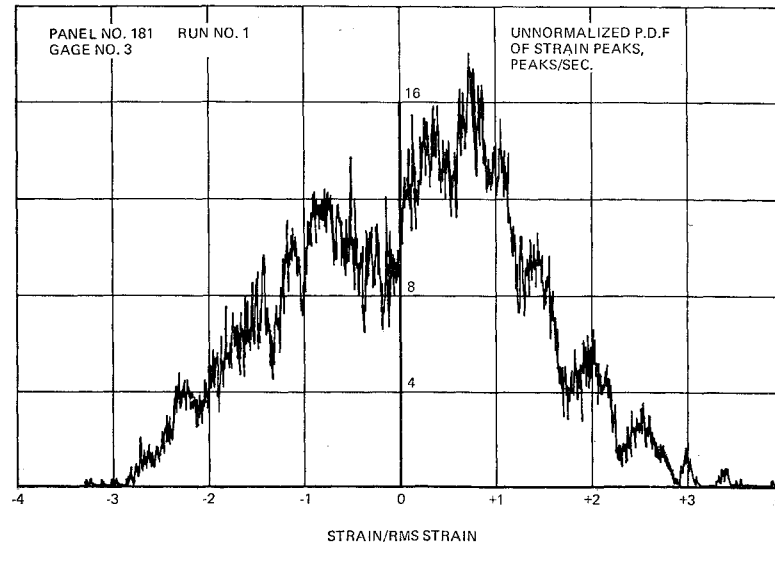

Fig. 7 Probability density function of positive and negative strain peaks at gage 3 of panel P3-181.

visual inspections were considered indispensable in detecting propagation of failures.

Strain gage failures occurred repeatedly during acoustic testing at maximum loading. Lead failures occurred most often early in the program. Taping the leads to the panel surface led to improved service from the leads so that in the later stages in the program, most strain gage failures were in the gages themselves. Sandblasting the panel surface with a No. 80 micron grit before applying the strain gages also proved beneficial in extending the strain gage life.

Experimental strain, natural frequencies, and damping data taken in the main acoustic test program are given in Table 3. Gage 1 (Table 3) was in the direction of flow at the center of honeycomb panels, and gage 2 was adjacent to gage 1 but perpendicular to the direction of the air flow in the progressive wave test chamber.

Types of Acoustic Failures

A brief summary of the acoustic fatigue test results is recorded in Table 1. Various modes of acoustic fatigue failures occurred. Facing cracks, delamination of facing-to-core because of adhesive failures, and core failures were all experienced. Facing cracks near the panel center were common for honeycomb panels with BFR facings; with aluminum alloy facings; and with S901/43 facings with either a 0°, 0° ply layup or a 0°, 90° ply layup. Facing cracks in SGFR and BFR facings, in general, propagated parallel to the principal elastic axis of a ply.

Core failures and/or delamination of a facing-to-core occurred along a long side (parallel to the flow direction) in 30 × 22-in. honeycomb panels with S901/81 facings and both 0°, 0° ply layup and −15°, 15° ply layup; and with S901/43

Table 3 Experimental strains, natural frequencies, and damping factors under loading at 139 db overall SPL

Panel	Strain						
	Gage No. 1		Gage No. 2			Damping factor	
	Discrete frequency, μ "/"	Random, μ "/"	Discrete frequency, μ "/"	Random, μ "/"	Fundamental frequency, Hz	Gage No. 1	Gage No. 2
A-1-1	382		369		147	0.036	0.038
A-1-2	254				137	0.037	
A-1-3	236	43			136	0.033	
A-1-4	388	52			130		
A-2-1	312	43			133	0.028	
A-2-2	198	38			125	0.058	
A-2-3	331	42	325	43	136	0.037	0.050
A-5-1	535	53	521	50	147	0.036	0.034
A-5-2	230	52			130	0.049	
A-5-3	216	36	235	38	137	0.050	0.032
B-1-1	111	43			108	0.067	
B-1-2	108	33	204	64	110	0.038	0.044
B-1-3	115		140	57	106	0.067	
B-4-1	37		66		123		
B-4-2	76	32			110	0.052	
C-1-1			159	61	107		0.049
C-4-1	90	34	166	62	111		0.045
C-4-2			153	70	97		
D-1-1			338		140	0.034	0.043
D-1-2	268				138	0.060	
D-1-3	382	56			137	0.036	
D-2-1	236	38	210	34	141	0.041	0.031
D-2-2	274	39			137	0.067	
E-1-1	98	34	146	53	110	0.047	0.034
E-1-2	89	38	127	59	113		
E-1-3	79	33			106		
E-2-1	97	38			112	0.023	
F-1-1	83	51	178	118	109		0.054
F-1-2	76	29					
F-2-1	68	31	117	51	105		
G-1-1			98	52	112		
G-1-2			166	57	116		0.039
G-1-3			134	39	109		
G-2-1			127	61	114		0.057
H-1-1	178	34	229	52	156	0.038	0.034
H-2-1	268	34	407	69	153	0.030	
H-3-1			318	45	156		0.027
I-1-1	305	41	338	46	147		0.042
I-1-2			337	41	160		0.066
I-2-1	258	59			152		
J-1-1	458	43	675	65	166	0.037	0.049
J-1-2	318	33	382	42	165	0.045	0.059
J-1-3	191	48			160	0.029	
K-1-1	42	18	94	43	130		0.028
K-1-2	71	20	166	43	122		0.050
K-1-3			108	41	119	0.028	
L-1-1	166	38	166	36	153	0.030	0.029
L-2-1	216	24			157	0.035	
L-3-1	268	26			165	0.014	

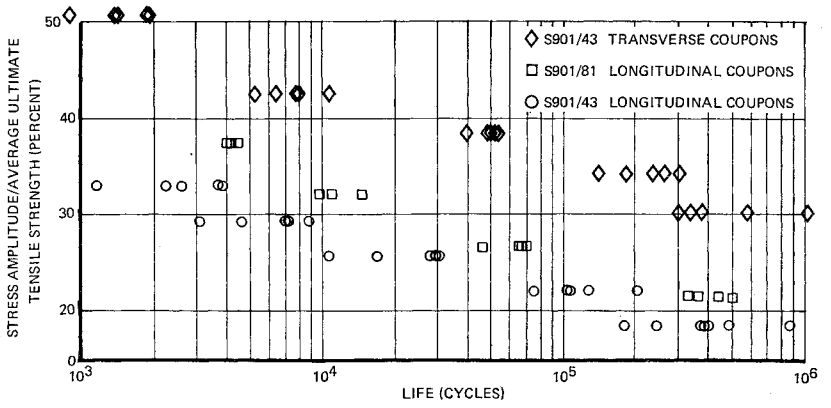

Fig. 8 Fatigue coupon test data.

facings with a $-15°$, $15°$ ply layup. Although the core failure probably occurred first, it was not conclusively determined that the core failures preceded the adhesive failures. Edge cracks caused failure only in a few of the acoustic fatigue tests. In most cases, the failure could be attributed to a too-sharp radius in the test fixture.

Coupon Fatigue Test Program

Description

Dogbone fatigue coupons 6 in. long by $1\frac{1}{2}$ in. wide by 27 ply thickness, of parallel plied SGFR laminates, were fabricated and cured in the same manner as the SGFR facings of the honeycomb panels. Three sets of coupons were fabricated; namely, the S901/43 transverse set (the uniaxial fatigue load being at a right angle to the warp direction of the laminate), the S901/81 longitudinal set (the uniaxial fatigue load being parallel to the warp direction of the laminate), and the S901/43 longitudinal set (the uniaxial fatigue load being parallel to the warp direction of the laminate). The fatigue tests were under fully reversed, discrete frequency, uniaxial loading, and the test results are given in Fig. 8. The average ultimate tensile strengths in the test program were 136.8 ksi for the S901/43L coupons, 93.8 ksi for the S901/81L coupons, and 26.6 ksi for the S901/43T coupons.

Statistical Observations

Because the usual number of coupons subjected to fatigue testing at a stress level was five, only a limited number of useful statistical results can be obtained from the coupon fatigue tests. Therefore, S-N curves, percent confidence level, and probability of survival are not presented. However, plots of probability of survival vs cycles were prepared, and they indicated a normal distribution at all stress levels for the coupons.

At the 25-ksi stress level, seven S901/43 longitudinal coupons were tested. The average number of kilocycles to failure was 426.31 with the minimum being 181.56 kc. For a 50% probability of survival with a 90% confidence level, the computed life to failure was 275 kc; and for a 90% probability of survival with a 90% confidence level, the computed life to failure was 138 kc.

The computed kilocycles to failure were obtained from

$$\log N = \log \bar{N} - K \log[\sum D_i/(n+1)]^{1/2}$$

with $K = 0.725$ for 90% confidence and 50% probability of survival for seven specimens, and $K = 2.3$ when the probability of survival is raised to 90%.

From Table 8 of an ASTM fatigue handbook[2], the probability of survival with a 50% confidence level at a stress above the initial failure (which was at 181.56 kc) is given as 87%.

Random S-N Curves

Random S-N curves have often been prepared based on: 1) the existence of a conventional S-N curve obtained under a constant loading rate and stress amplitude; 2) the applicability of Miner's law of cumulative damage; 3) the existence of a Rayleigh probability of strain peaks in random loading.

Random S-N curves have been prepared using the above method for the S901/43 transverse coupons, the S901/81 longitudinal coupons, and the S901/43 longitudinal coupons and are presented in Fig. 9. For the random S-N curve, first a conventional S-N curve was drawn through the test points in Fig. 5 representing the minimum cycles to failure for a given material and warp direction in order to comply with the preceding category 1. This may or may not be considered a conservative approach to the problem since it was just shown that, for the S901/43 longitudinal specimens at a 25-ksi stress level, the probability of survival past 181.56 kc was 87% with a 50% confidence level.

Comparison of Fatigue Lives of Honeycomb Panels and Nonhoneycomb Coupons

Each of the SGFR fatigue coupons was fabricated with parallel-plied laminae. The honeycomb panels with SGFR facings had either parallel-plied laminae, angle-plied laminae, or cross-plied laminae. The coupons were loaded only unidirectionally, whereas the facings of the honeycomb panels experienced biaxial loading.

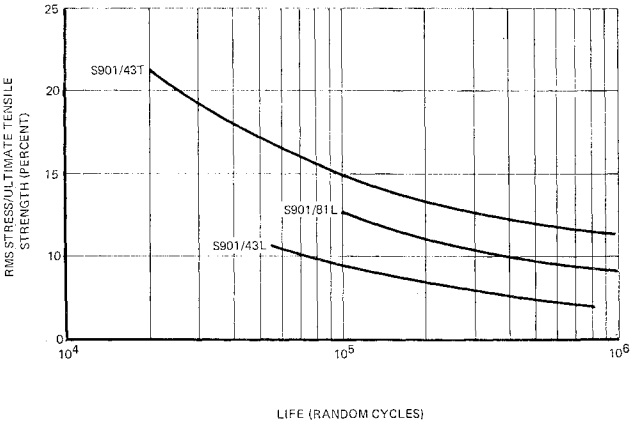

Fig. 9 Tentative random S-N curves for parallel-plied fiber glass laminates.

Data are presented in Table 4 for honeycomb panels that experienced facing cracks near the panel center. The failures propagated mainly parallel to the warp direction of the SGFR plies and parallel to the seams of the boron tape. For SGFR facings, S_L and S_T relate to the warp direction and fill direction, respectively; for BFR facings, S_L and S_T relate to the filament and transverse directions, respectively. Experimental stresses $S_{L\text{-EX}}$ and $S_{T\text{-EX}}$ of the surface ply were computed on the basis of strain data (sometimes estimated) at gages at the center of the panel in the direction (gage 1) and perpendicular to the direction (gage 2) of flow in the progressive wave acoustic test chamber. The experimental life in the last column of Table 4 is a product of the known experimental fundamental frequency and the test time from the preceding two columns.

The theoretical stress $S_{T\text{-TH}}$ (in Table 4) at failure of the honeycomb panels with SGFR facings subjected to discrete frequency loading was obtained from the life in the last column of Table 4 and the corresponding stress in Fig. 8. The theoretical stress $S_{T\text{-TH}}$ at failure under random loading was obtained from the life in the last column of Table 4 and the corresponding stress in Fig. 9. Theoretical stresses $S_{T\text{-TH}}$ were not prepared for the BFR facings because of the unavailability of coupon fatigue data.

In every instance in Table 4, the experimental stress $S_{T\text{-EX}}$ for honeycomb panels with SGFR facings is less than the theoretical stress $S_{T\text{-TH}}$. This can be attributed to the fact

Table 4 Approximate stress and strain at the panel center and the expected stress at failure due to facing cracks

Panel	Type of load	Approximate experimental strain, rms[a] Gage No. 1 μ"/"	Gage No. 2 μ"/"	Approximate experimental stress, rms $S_{L\text{-EX}}$,[b] ksi	$S_{T\text{-EX}}$,[c] ksi	Theoretical stress at failure[d] rms, $S_{T\text{-TH}}$,[c] ksi	Approximate frequency,[a] Hz	Estimated experimental time to failure, min	Estimated experimental life, kc
A-1-6	DF[e]	1650	1650	8.0	7.4	12.9	155	75	698
D-1-1	DF	1370	1270	8.7	4.1	6.3	161	10	97
D-1-3	DF	1370	1270	8.7	4.1	6.1	161	15	145
D-2-1	R[f]	770	700	4.8	2.3	2.9	145	300	2610
E-1-1	DF	1170	1340	9.0	3.6	5.8	124	30	223
E-1-2	DF	1170	1340	9.0	3.6	6.7	120	7	50
E-1-3	DF	1170	1340	9.0	3.6	6.5	119	10	71
E-2-1	R	700	900	6.0	2.2	3.4	118	150	1162
E-2-2	R	700	900	6.0	2.2	3.4	118	130	920
E-2-3	R	700	900	6.0	2.2	3.4	118	150	1162
H-2-1	R	318	484	11.4	2.0		153	4	37
J-1-1	R	713	930	25.8	4.1		175	18	189
J-1-2	R	572	738	20.7	3.2		175	12	126
J-1-3	R	585	750	21.2	3.3		175	18	189
K-1-2	R	445	965	18.3	3.7		135	120	972
L-1-1	DF	985	985	15.8	15.8	22.2	177	4	42
L-2-1	R	560	560	9.0	9.0		165	150	1485
L-3-1	DF	852	852	13.7	13.7	13.0	182	39	424

[a] Estimated in some instances.
[b] S_L = stress in the warp direction of S-glass ply or in the filament direction in boron ply. $S_{L\text{-EX}}$ = experimental S_L.
[c] S_T = in-plane facing stress perpendicular to S_L. $S_{T\text{-TH}}$ = theoretical S_T. $S_{T\text{-EX}}$ = experimental S_T.
[d] The theoretical stresses S_T given in this column are obtained from S-N curves (see Fig. 8 for discrete frequency excitation and Fig. 9 for random excitation of honeycomb panels with SGFR facings) and the experimental life in the last column of this table.
[e] DF = discrete frequency.
[f] R = random.

Table 5 Experimental stress at the center of selected honeycomb panels that did not experience facing cracks at the panel center

Panel	Type of load	Approximate experimental strain, rms[a] Gage No. 1 μ"/"	Gage No. 2 μ"/"	Approximate experimental stress, rms $S_{L\text{-EX}}$,[b] ksi	$S_{T\text{-EX}}$,[c] ksi	Approximate frequency,[a] Hz	Time to end of test, min	Life at end of test, kc
A-5-3	R[d]	876	865	4.3	3.9	145	500	4350
B-1-1	DF[e]	840	1270	6.0	4.0	120	500	3600
B-1-2	DF	1020	1590	7.5	4.8	118	11	78
B-1-3	DF	1528	1462	7.2	6.8	118	500	3540
B-4-1	R	1043	1594	7.5	4.9	120	500	3600
B-4-2	R	661	990	4.7	3.1	115	500	3450
C-4-1	R	712	966	4.6	3.4	113	500	3390
F-1-1	DF	1144	1848	10.1	4.6	115	500	3450
F-1-2	DF	1122	1800	9.9	4.5	122	500	3660
F-2-1	R	547	685	4.2	1.9	111	500	3330
G-2-1	R	547	775	5.0	1.8	112	101	678
I-1-1	R	650	687	24.0	3.1	159	500	4760
I-1-2	R	700	738	25.7	3.3	159	500	4760
I-2-1	DF	1350	1380	48.3	6.4	171	500	5130
K-1-1	R	432	763	16.8	3.0	145	500	4350
K-1-3	R	775	1370	31.2	5.5	130	500	3900

[a] Estimated in some instances.
[b] S_L = stress in the warp direction of S-glass ply or in the filament direction of boron ply. $S_{L\text{-EX}}$ = experimental S_L.
[c] S_T = in-plane facing stress perpendicular to S_L. $S_{T\text{-EX}}$ = experimental S_T.
[d] R = random.
[e] DF = discrete frequency.

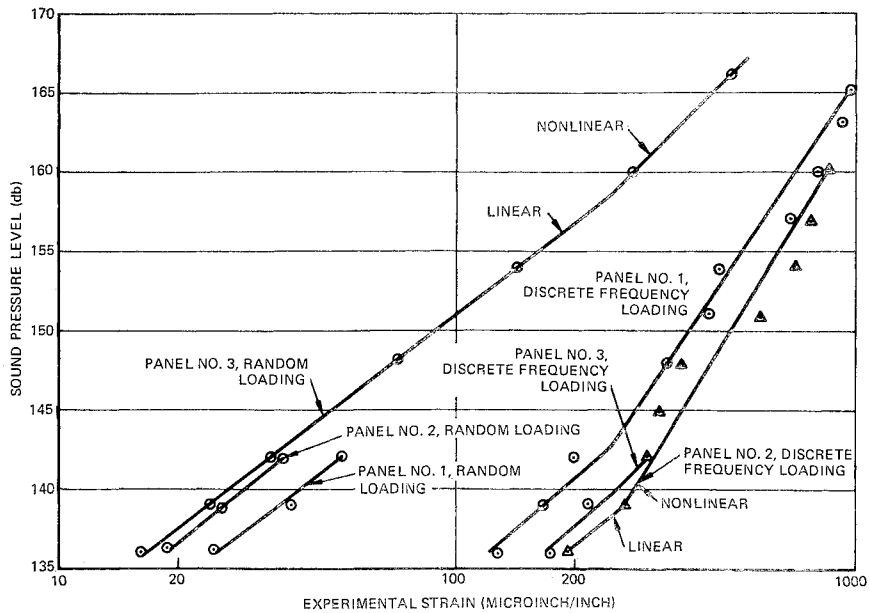

Fig. 10 Strain response to acoustic loading of three aluminum honeycomb panels.

that the experimental stress $S_{T\text{-EX}}$ is part of a biaxial stress state in the panels and is being compared to the theoretical stress $S_{T\text{-TH}}$ obtained from S-N curves (Fig. 8 or Fig. 9) that resulted from uniaxial testing. Therefore, the theoretical stresses $S_{T\text{-TH}}$ would have been poor choices for allowable stresses in the honeycomb panels with SGFR facings if the required panel life-time had been specified by the last column of Table 4.

In Table 5 are recorded the experimental stresses $S_{L\text{-EX}}$ and $S_{T\text{-EX}}$ at the panel center and the number of kilocycles in testing that did not culminate in a facing failure at the panel center. Therefore, the experimental stresses $S_{L\text{-EX}}$ and $S_{T\text{-EX}}$ in Table 5 and the life at the end of the test represent a lower bound on the life at the stress state, S_L and S_T.

In all the calculations for Tables 4 and 5 leading to experimental stresses $S_{L\text{-EX}}$ and $S_{T\text{-EX}}$, the shear strain in the direction defined by strain gages 1 and 2 at the panel center was assumed zero. In some instances this was verified experimentally and no significant violation of the assumption was observed.

The stresses $S_{L\text{-EX}}$ and $S_{T\text{-EX}}$ were only partially responsible for failure since honeycomb panels F-1-1 and F-1-2 (S901/43 facings with a $-45°$, $45°$ ply layup) experienced higher stresses $S_{L\text{-EX}}$ and $S_{T\text{-EX}}$ without failure than panels D-1-1 and D-1-3 (S901/43 facings with a $0°$, $0°$ ply layup) experienced at failure (Tables 4 and 5).

Stress Predictions under Acoustic Loading

The theory developed in Ref. 1 was limited to the linear response of honeycomb panels, simple supported on all edges, with orthotropic facings that were thin relative to the thickness of an orthotropic core. The validity of the assumptions of linear response, of simple supports, and of orthotropic facings will now be discussed.

Strain gage data observed under acoustic pressures up to 168 db showed a nonlinear strain-load relation at the load levels that led to acoustic fatigue failures. Figures 10 and 11 illustrate the nonlinear response of 22 × 22-in.-square honeycomb panels under either discrete frequency loading or random loading. The strain response obtained with strain gages is essentially a linear function of load until a certain level is reached (in Fig. 10, Panel No. 1 is Panel L-1-1; Panel No. 2 is Panel L-3-1; and Panel No. 3 is Panel L-2-1. In Fig. 11, Panel No. 1 is Panel A-2-2 and Panel No. 2 is Panel A-5-3).

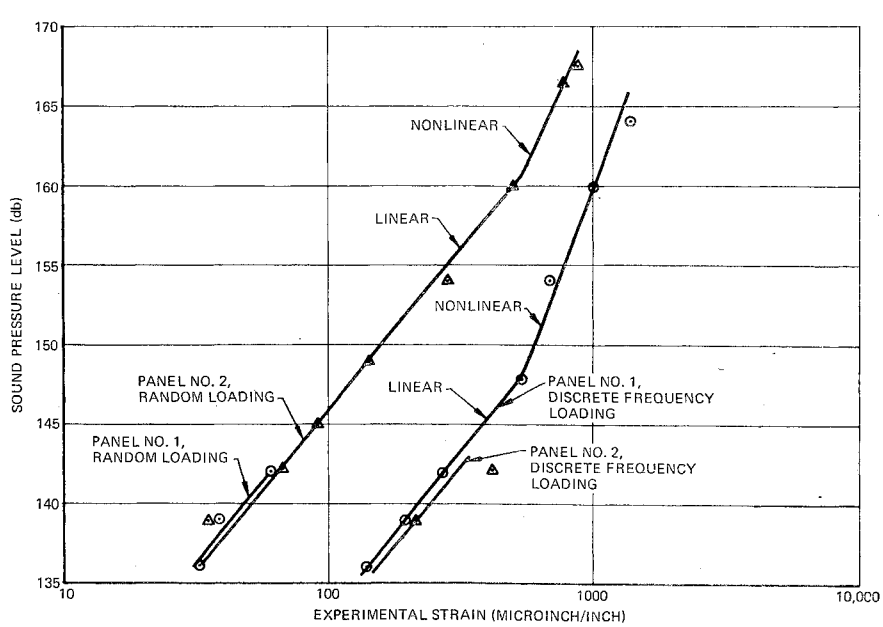

Fig. 11 Strain response to acoustic loading of two honeycomb panels with S-glass fabric facings.

Consequently, the linear theory was of little value in predicting the strain response at the load levels causing fatigue failures; however, in general satisfactory agreement was reported[1] between experimental and theoretical strain response at the panel center at low load levels where linear theory was applicable.

Although the experimental boundary conditions were not simple supports, a satisfactory method of estimating effective edge lengths to be used in strain and stress predictions at the panel center of simply supported panels was available. The method consisted of estimating effective edge lengths of a simply supported panel from the known experimental fundamental frequency.

The conditions required for an orthotropic facing were satisfactory in the parallel-plied and cross-plied facings. It was demonstrated[1] analytically that, although the angle-plied facings were not orthotropic, the errors introduced due to the orthotropic assumption for the facings were insignificant since the facings were so thin.

From the outset, a program objective was the prediction of honeycomb panel fatigue life based on stress data. Because of the nonlinear experimental response, the method of predicting stress at the load levels causing failure was unsatisfactory. At present, there is no satisfactory theoretical way of predicting the nonlinear stress response from acoustic loading of panels with arbitrary boundary conditions. The development of such theory will, of course, be useful.

Because, in the linear response range, agreement between the experimental and theoretical stress at the panel center was satisfactory, the simplified formulas developed in Sec. V of Ref. 1 for the strain and stress at the panel center and for the fundamental frequency for use in preliminary design may be used. The formulas are limited to cases where 1) linear theory (stress-strain and strain-displacement relations) is applicable; 2) the acoustic pressure is characterized by a power spectral density that is uniform in space and in frequency content; 3) the response is unimodal at the fundamental frequency; 4) the core is isotropic, i.e., cores with core shear moduli equal in the ribbon and transverse direction; 5) the two facings are identical and are either parallel-plied, angle-plied, or cross-plied. It is recommended that the simplified formulas be used only in preliminary design when configurations are being sought, and that more exact formulas such as used in the computer program reported in Ref. 1 be used in establishing the final design so that restrictions such as an isotropic core and unimodal response may be lifted.

Numerical results using the simplified formulas differ from the computer results by about 3% due to the assumption of the isotropic core. A difference of about 3% was anticipated as a result of a previous analysis[3] on the effects of orthotropic cores on the free vibrations of aluminum honeycomb plates.

Once the stresses at the panel center have been calculated or estimated in some other manner, the designer is referred to Fig. 9 and Tables 4 and 5 for guides in predicting fatigue life.

Results and Conclusions

The test program was formulated to assess a two-step life prediction method in which, in the first step, the stress state at the panel center is predicted, and, in the second step, the panel life (on the assumption that failure will occur at the panel center) is estimated using the predicted stress and S-N curves. The experimental program and data analysis have demonstrated that the above method does have merit. Precautions in using the above two-step method include 1) the consideration of nonlinear strain-deflection relations in predicting stress in step 1, and 2) the modification of S-N curves obtained under unidirectional loading of fatigue coupons to account for the biaxial stress state at the center of panels under acoustic loading.

The use of the elementary Rayleigh-Minor hypothesis for obtaining random S-N curves from fatigue coupons under constant-amplitude discrete-frequency unidirectional loading appears to be satisfactory since the ratio of the experimental $S_{T\text{-EX}}$ and theoretical $S_{T\text{-TH}}$ in Table 4 are of the same order of magnitude for discrete frequency and random loading. A major reason why the aforementioned ratio is not unity is the biaxial stress state in the panels.

The strain gage data taken under acoustic loading with increasing intensity indicated that nonlinear strain-deflection relations existed at the load levels causing acoustic fatigue failures. There is no generally accepted theory with nonlinear strain-deflection relations for acoustic loading of the honeycomb panels and, therefore, one must be developed in order to satisfy step one of the two-step life prediction method without resorting to empirical means. As a result of neglecting the nonlinear effects, the stresses based on the linear stress-load formulas are unrealistically high, and therefore lead to a panel design that is unduly conservative.

In the design of honeycomb panels, the question of preferable mode of failure has not been resolved. The preferable mode is defined as the mode which does not lead to an instant or sudden catastrophic panel failure. In-service catastrophic failures are undesirable, and greater margins of safety are required when a catastrophic failure is a possibility. Whether a facing failure is more apt than a core failure to lead to a sudden catastrophe is of concern to designers. The rates of propagation of the facing failures and of the core failures reported in Table 1 show that facing failures in honeycomb panels with SGFR facings did not propagate at a rate much different than core and adhesive failures propagated. More experimental work is required to establish propagation rates-to-failure of different modes of failure. If it should be established that a core failure is the preferable mode of failure, then more attention should be given to design criteria where a core failure is the failure mode. Furthermore, criteria are needed for adhesives to avoid adhesive failures.

From the linear theory in Appendix II of Ref. 1, one cannot predict that the core shear stresses in the rectangular panels with the $-15°$, $15°$ ply layup (the C-series and the G-series) are more critical than the core shear stresses in the other rectangular panels (the B-series, the E-series, and the F-series). However, core shear failures apparently occurred with regularity in C- and G-series panels but not in the other panels. Therefore, more investigations are required to ascertain the effects of ply layups on core failures.

Acoustic fatigue design criteria for fiber-reinforced structure are in a formative stage. This paper presents design guidelines that are useful at the present level of the state-of-the-art. All of the acoustic tests of the honeycomb panels with SGFR facings were limited to panels with two-ply facings that were either angle-plied, cross-plied, or parallel-plied. Caution should be exercised in extending the program results to panels with thicker facings. Additional testing and analysis are required for the general case of a sandwich structure with multiplied fiber-reinforced facings (e.g., with glass, boron, or graphite fibers) because of the many variables, which include an arbitrary orientation of plies in a facing, the twist-pull coupling effect in a thick facing, the dependence of the orthotropic properties and strength of a facing on the resin system and method of cure, the variability of orthotropic properties and strength of a facing on the resin system and method of cure, the variability of orthotropic properties of core materials, and a lack of detailed knowledge of the actual mechanism of failure under acoustic loading.

Appendix: Auto and Cross Correlation of the Pressure

The auto correlation coefficient of $f_i(t)$ is defined as:

$$R_i(\tau) = \frac{\int_0^\infty f_i(t) f_i(t+\tau) dt}{f_{t_{\text{rms}}}{}^2} \tag{A1}$$

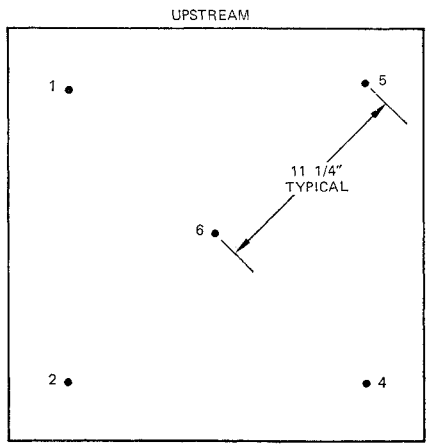

Fig. 12 Microphone locations (24 × 24-in. test cell) for auto and cross correlation of pressure under random excitation.

Auto and cross correlations of the pressure were obtained for five microphone locations (Fig. 12) in the concrete plug at the 24 × 24-in. test cell of the progressive wave test chamber. These correlations determined the characteristics of the uniformity of the pressure at the 24 × 24-in. test cell. Typical auto and cross correlations for this area at an SPL of 139 db are presented in Figs. 13 and 14. The distance between the center of the central microphone and the center of each of the other microphones was about 11.25 in. The pressure was obtained using Photocon 524–5 microphones conditioned by a DG-605D Dyna Gage and recorded on a Sanborn 3914 magnetic recorder. The data were analyzed with the Honeywell 9410 Time Delay Correlation.

Sound propagates downstream in the progressive wave acoustic test chamber at approximately 1100 fps or 13 in./msec.

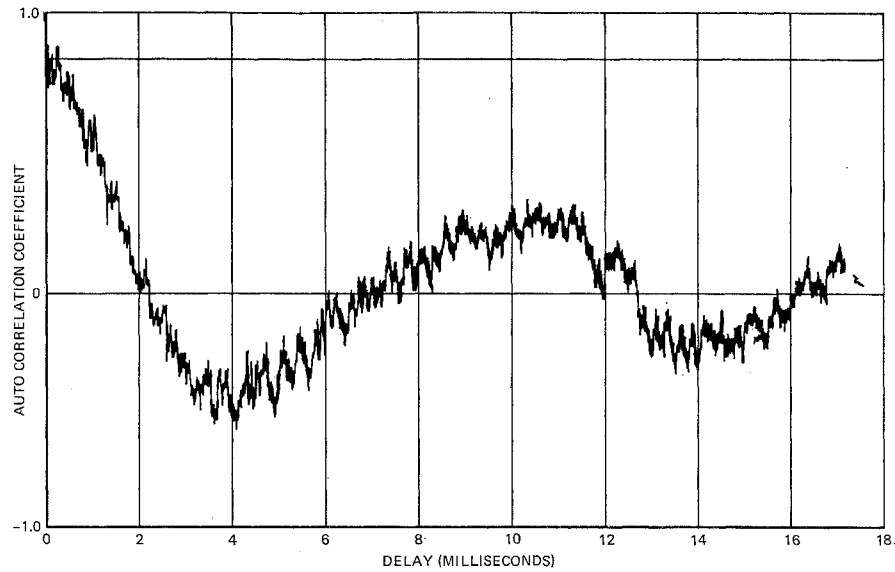

Fig. 13 Auto correlation of pressure at microphone 6 at 139 db SPL (24 × 24-in. test cell).

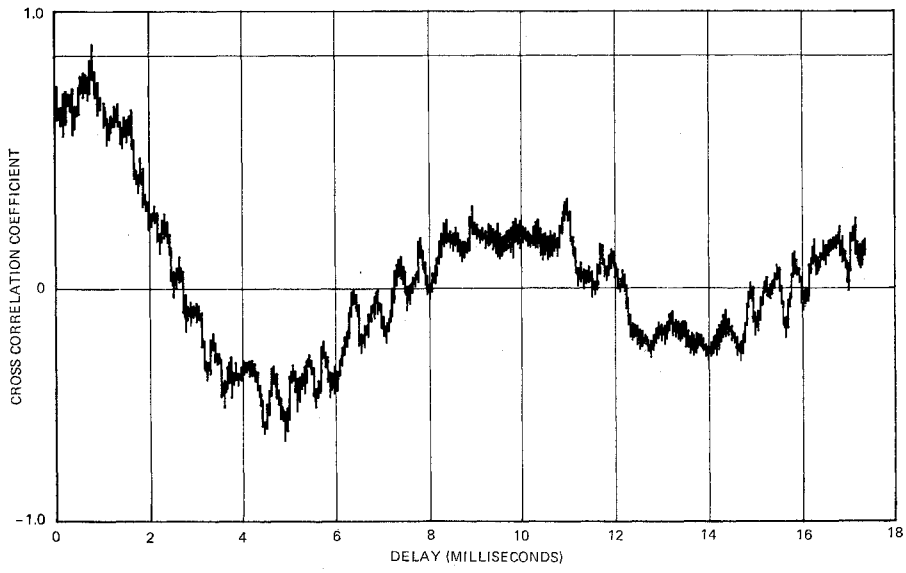

Fig. 14 Cross correlation of pressure at microphones 6 and 2 at 139 db SPL (24 × 24-in. test cell).

and the cross correlation coefficient of $f_i(t)$ is defined as:

$$R_{ij}(\tau) = \frac{\int_0^\infty f_i(t) f_j(t+\tau) dt}{f_{i\text{rms}} f_{j\text{rms}}} \qquad \text{(A2)}$$

For the 24 × 24-in. test cell, the time required for a pressure signal to move from the chamber cross section at the upstream microphone location 1 or 5 to the chamber cross section at the central microphone location 6 was 0.60 msec, which was

also the time required in moving from the chamber cross section at the central microphone location 6 to the chamber cross section at the downstream microphone location 2 or 4. From the figures, the cross correlation of the pressure between the central location 6 and any of the other locations can be seen to peak, in general, at approximately unity with a delay ranging between 0.4 and 0.8 msec, which compares satisfactorily with the theoretical period of 0.6 msec for no signal distortion.

For the 24 × 24-in. test cell, the cross correlation figures, in general, show good correlation (i.e., approximately unity) with no time delay between the pressures at the various microphone locations and are reported in Ref. 4.

Auto and cross correlation curves at nine locations (Fig. 15) of the 48 × 48-in. test cell of the progressive wave test chamber have been obtained and are reported in Ref. 5.

The cross correlation curves of Refs. 4 and 5 in conjunction with experimental or theoretical periods of free vibration have been used to justify the assumption of approximately spatial uniformity of acoustic pressure applied to panels in the 24 × 24-in. and 48 × 48-in. test cells when the periods of free vibration of the modes being excited are much greater than the time required for sound propagation across the panel.

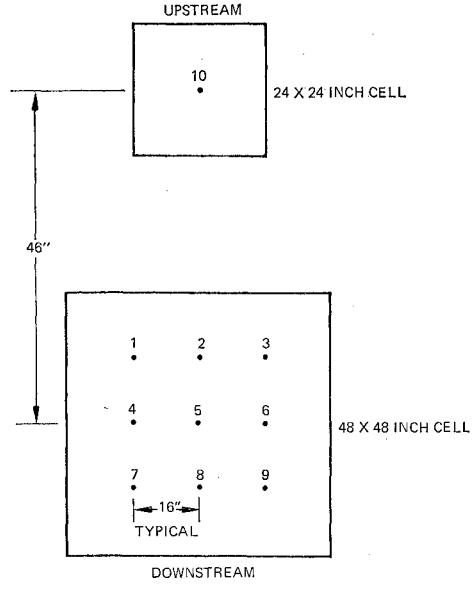

Fig. 15 Microphone locations for auto and cross correlation of pressure.

References

[1] Jacobson, M. J., "Acoustic Fatigue Design Information for Fiber-Reinforced Structures," TR AFFDL-TR-68-107, Oct. 1968, Wright-Patterson Air Force Base, Ohio.

[2] "A Guide for Fatigue Testing and the Statistical Analysis of Fatigue Data," *ASTM Special Technical Publication No. 91-A*, 2nd ed., 1963, ASTM, Philadelphia, Pa.

[3] Jacobson, M. J., "Effects of Orthotropic Cores on the Free Vibrations of Sandwich Plates," *The Shock and Vibration Bulletin*, No. 35, Pt. 3, Jan. 1966, pp. 9–14.

[4] Jacobson, M. J., Acoustic Fatigue Design Information for Skin-Stiffened Metallic Panels," Rept. NOR 69–111, Aug. 1969, Northrop Corp., Hawthorne, Calif.

[5] Jacobson, M. J., "Dynamic Response and Acoustic Fatigue Characteristics of Flat Skin-Stringer Aluminum Alloy Panels," Rept. NOR 70–22, Feb. 1970, Northrop Corp., Hawthorne, Calif.